

EOM-CC guide for Fock space travel: The C₂ edition

Sahil Gulania^a, Thomas-C. Jagau^b and Anna I. Krylov^{a,c}

^a Department of Chemistry, University of Southern California, Los Angeles, California 90089, USA

^b Department of Chemistry, University of Munich (LMU), 81377 Munich, Germany

^c The Hamburg Centre for Ultrafast Imaging, Luruper Chaussee 149, 22671 Hamburg, Germany

Despite their small size, C₂ species pose a big challenge to electronic structure owing to extensive electronic degeneracies and multi-configurational wave functions leading to a dense manifold of electronic states. We present detailed electronic structure calculations of C₂, C₂⁻, and C₂²⁻ emphasizing spectroscopically relevant properties. We employ double ionization potential (DIP) and ionization potential (IP) variants of equation-of-motion coupled-cluster method with single and double substitutions (EOM-CCSD) and a dianionic reference state. We show that EOM-CCSD is capable of describing multiple interacting states in C₂ and C₂⁻ in an accurate, robust, and effective way. We also characterize the electronic structure of C₂²⁻, which is metastable with respect to electron detachment.

I. INTRODUCTION

Ironically, the smallest form of neat carbon, the C₂ molecule, features the most complex electronic structure. The complexity stems from the inability of four valence electrons of carbon to form a quadrupole bond (remarkably, the bonding in C₂ is still hotly debated¹⁻⁸). Because the optimal electron pairing cannot be reached, multiple electronic configurations have similar likelihood, leading to a dense manifold of low-lying electronic states. This results in rich spectroscopy: C₂ features multiple low-lying electronic transitions, which have been extensively studied experimentally⁹⁻¹⁴. Despite a long history of experimental work, C₂ continues to generate interest. For example, recently new band systems have been identified¹⁵⁻¹⁷.

Besides obvious fundamental importance, C₂ (and its anionic forms, C₂⁻ and C₂²⁻), play a role in combustion¹⁸, plasma¹⁹⁻²¹, and astrochemistry^{19,22}. For example, C₂ and C₂⁻ have been observed in comet tails, protoplanetary nebulae, the atmospheres of stars, and in the diffuse interstellar medium²²⁻²⁷. C₂ is responsible for the color of blue flames¹⁸. It is also a

prominent product of electrical discharges containing hydrocarbons²⁰.

From the theoretical point of view, C_2 is arguably the most difficult molecule among homonuclear diatomics from the first two rows of the periodic table. Electronic near-degeneracies lead to multiconfigurational wave-functions. Small energy separations between different electronic states also call for high accuracy. Because of its complex electronic structure, C_2 has been often described as a poster child of multi-reference methodology. The availability of high-quality spectroscopic data, complex electronic structure, and its small size make C_2 a popular benchmark system for quantum chemistry studies²⁸⁻³². Among recent theoretical studies of the low-lying states of C_2 , the most comprehensive are tour-de-force MR-CISD (multi-reference configuration interaction with single and double excitations) calculations by Schmidt and coworkers³³ and by Szalay and co-workers³⁴. In both studies, the effect of basis set and higher-order corrections have been carefully investigated. To correct MR-CISD energies for violation of size-extensivity, Davidson’s quadruple correction was used. Szalay and co-workers have also reported results obtained with an alternative strategy, the so-called MR-average quadratic coupled-cluster (AQCC) method. In both studies, the theoretical values of the reported equilibrium distances (r_e) and term energies (T_{ee}) agreed well with the experimental data.

The anionic forms of C_2 , C_2^- and C_2^{2-} , have received less attention. C_2^- is produced in plasma discharge from acetylene^{35,36}. Electronically excited C_2^- has been observed in a carbon-rich plasma via fluorescence²¹. Recently, C_2^- has been proposed as a candidate for laser cooling of anions³⁷, which makes these species interesting in the context of quantum information storage. Ervin and Lineberger³⁸ have measured photoelectron spectrum of C_2^- using 3.53 eV photons; they reported adiabatic electron affinity (AEA) of C_2 to be 3.269 ± 0.006 eV. A similar value (3.273 ± 0.008 eV) has been derived by Neumark and coworkers³⁹, who reported vibrationally resolved photodetachment spectra using 4.66 eV radiation. Feller has reported an AEA of 3.267 eV calculated using a composite method based on coupled-cluster (CC) methods⁴⁰.

Because of the highly unsaturated character of C_2 , it has relatively large electron attachment energy so that even the two lowest excited states of C_2^- are bound electronically. In contrast, C_2^{2-} is metastable with respect to electron detachment. Its existence has been postulated on the basis of features observed^{41,42} in electron scattering from C_2^- and confirmed by calculations^{43,44}.

In this contribution, we present detailed electronic structure calculations of C_2 , C_2^- , and C_2^{2-} , with an emphasis on spectroscopically relevant properties. We employ an alternative methodology based on CC and equation-of-motion CC (EOM-CC) theory^{45–49}. We show that electronic states of C_2 and C_2^- are well described by the double ionization potential (DIP)⁵⁰ and ionization potential (IP)^{51,52} variants of EOM-CCSD (EOM-CC with single and double substitutions) using a dianionic reference state. Formulated in a strictly single-reference fashion, the EOM-CC family of methods provides an accurate, robust, and effective alternative to cumbersome multi-reference calculations^{45–49}. To describe metastable species, such as C_2^{2-} , we employ the complex-variable extension of CCSD and EOM-CCSD via the complex absorbing potential (CAP) approach^{53–55}.

II. MOLECULAR ORBITAL FRAMEWORK AND ESSENTIAL FEATURES OF ELECTRONIC STRUCTURE OF C_2 SPECIES

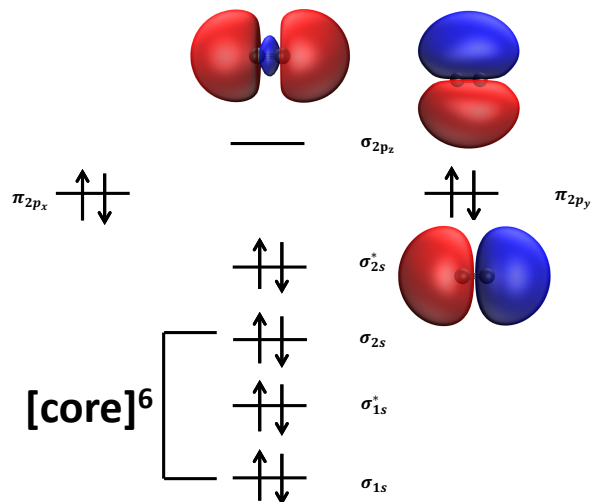


FIG. 1: Molecular orbital diagram. The three lowest orbitals that remain doubly occupied in the low-energy manifold of electronic states of C_2 and C_2^- are denoted as ‘core’. The electronic states of C_2 are derived by distributing six additional electrons over four upper orbitals, σ_{2s}^* , π_{2px}/π_{2py} , and σ_{2pz} . Shown is the leading electronic configuration of the ground state, $X^1\Sigma_g$. Low-lying states of C_2^- are derived by distributing five electrons over the four upper orbitals. In C_2^{2-} , all four upper orbitals are doubly occupied. Shown are Dyson orbitals (isovalue = 0.05) computed with EOM-IP-CCSD/aug-cc-pVTZ from the dianionic reference.

Fig. 1 shows the molecular orbital diagram and describes orbital occupation patterns in C_2 , C_2^- , and C_2^{2-} . Due to orbital near-degeneracies, various electronic configurations of six electrons over the upper four orbitals have similar energies, leading to closely lying electronic states and multi-configurational wave-functions. In C_2^- , there are four important configurations in which the unpaired electron resides on one of the upper orbitals. In C_2^{2-} , which is isoelectronic with N_2 , all four upper orbitals are doubly occupied, resulting in the electronic configuration $[core]e^6(\sigma_{2s}^*)^2(\pi_{2px})^2(\pi_{2py})^2(\sigma_{2pz})^2$. Consequently, the ground state of C_2^{2-} is a well-behaved closed-shell state dominated by a single Slater determinant; thus, it can be well described by single-reference methods such as, for example, CCSD. From this reference state, EOM-IP and EOM-DIP operators can generate all important electronic configurations needed for describing the electronic states of C_2^- and C_2 , respectively, as illustrated in Fig. 2.

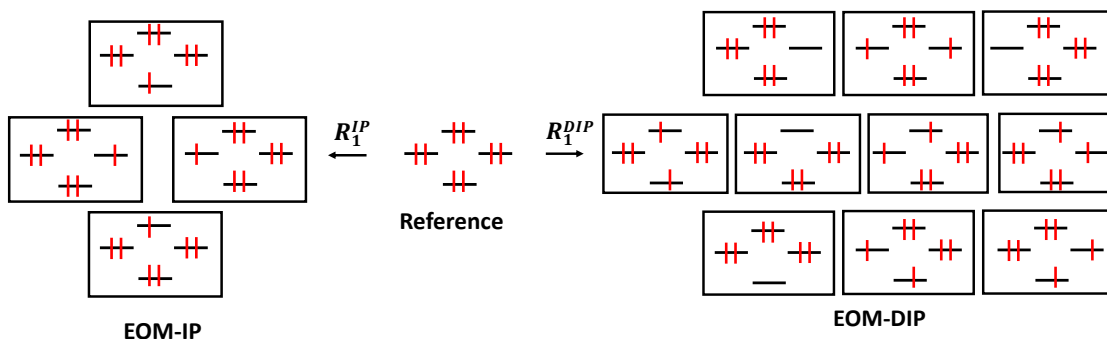


FIG. 2: EOM-IP (left) and EOM-DIP (right) manifolds generated from the dianionic reference (center). Only configurations generated by \hat{R}_1 from the top four orbitals from Fig. 1 are shown. EOM-IP enables access to the ground and electronically excited states of C_2^- , whereas EOM-DIP describes the ground and excited states of C_2 .

Mathematically, the EOM-CCSD target states are described by the following ansatz^{46–48}:

$$\Psi = (\hat{R}_1 + \hat{R}_2)e^{\hat{T}_1 + \hat{T}_2}\Phi_0, \quad (1)$$

where $e^{\hat{T}_1 + \hat{T}_2}\Phi_0$ is the reference CCSD wave function (the amplitudes of the excitation operator \hat{T} are determined by the CCSD equations for the reference state) and operator \hat{R} is a general excitation operator. In EOM-IP-CCSD, \hat{R} comprises all $1h$ (one hole) and $2h1p$ (two hole one particle) operators^{51,52}, whereas in EOM-DIP-CCSD it includes all $2h$ and $3h1p$ operators. In EOM-EE-CCSD (EOM-CCSD for excitation energies⁵⁶) and EOM-SF-CCSD

(spin-flip EOM-CCSD^{57,58}), \hat{R} is particle-conserving and includes $1h1p$ and $2h2p$ operators (in the SF variant, \hat{R} changes the number of α and β electrons). In the EA (electron attachment) variant⁵⁹, the operator R is of the $1p$ and $1h2p$ type. The amplitudes of \hat{R} are found by diagonalization of the similarity-transformed Hamiltonian, \bar{H} :

$$\bar{H} = e^{-T} H e^T, \quad (2)$$

$$\bar{H} R^k = E_k R^k. \quad (3)$$

Linear parameterization ensures that different configurations can mix and interact. There are no assumptions about their relative importance—the relative weights of different configurations are defined by the EOM eigen-problem and can span the entire range of situations, from the cases dominated by a single electronic configuration to the cases of equal contributions from multiple determinants. The EOM-CC ansatz is capable of reproducing exact degeneracies (such as between the two components of Π states in linear molecules or Jahn-Teller degeneracies), which are violated by state-specific MR treatments. Since all important configurations appear at the same excitation level, they are treated in a balanced way. As a multi-state method, EOM-CC produces the entire manifold of electronic states, without requiring user input regarding state character. These features of EOM-CC make it very attractive for treating multiple electronic states and extensive degeneracies⁴⁹. Among recent applications illustrating the power of EOM-CC, we mention calculations of electronic states of copper oxide anions⁶⁰, Cvetanović diradicals⁶¹, and molecules with several unpaired electrons^{62,63}.

The success of EOM-CC in treating a particular electronic structure depends on whether a proper well-behaved reference can be found from which the target-states manifold can be reached by an appropriately chosen \hat{R}_1 . As illustrated in Fig. 2, the electronic structure of C_2 is best described by EOM-DIP using the dianionic reference state. The DIP method is capable of describing electronic degeneracies beyond two-electrons-in-two-orbitals or three-electrons-in-three-orbitals patterns^{50,60,61,64–68}, however, its applications are limited by the complications due to the use of the dianionic reference.

Isolated dianions of small molecules are usually unstable with respect to electron detachment and exist only as transient species.⁶⁹ In dianions, the competition of long-range repulsion between an anionic core and an extra electron versus stabilizing valence interactions with short-range character leads to a repulsive Coulomb barrier. The extra elec-

tron is trapped behind this barrier but can leave the system by tunneling. This is similar to metastable radical monoanions where the extra electron is trapped behind an angular-momentum barrier also affording resonance character. In a computational treatment using a sufficiently large basis, the wave function of a resonance becomes more and more diffuse, approximating a continuum state corresponding to an electron-detached system and a free electron^{70–72}.

Resonances can be described by a non-Hermitian extension of quantum mechanics⁷³ by using, for example, complex absorbing potential (CAP)^{74,75}. If one is interested in the dianionic state itself, then the CAP-based extension of CC theory can be used⁵⁵. However, in practical calculations using EOM-DIP-CC, the dianionic state just serves as a reference for generating target configurations. Thus, less sophisticated approaches can be used to mitigate complications due to its metastable character. The easiest and most commonly used one is to use a relatively small basis set, such that the reference state is artificially stabilized^{50,60,61,64–66,76}. Kuś and Krylov have investigated an alternative strategy, stabilization of the resonance using an artificial Coulomb potential with a subsequent de-perturbative correction^{71,72}. Here we show that in the case of C_2 using the aug-cc-pVTZ basis provides a robust description of the dianionic reference, delivering accurate results for the target states. To further validate these calculations, we carried out CAP-EOM-IP-CCSD calculations in which the dianionic reference is stabilized by the CAP and compare the potential energy curves of C_2^{2-} and C_2^- obtained by these two calculations.

In the CAP approach^{74,75}, the Hamiltonian is augmented by a purely imaginary confining potential $i\eta W$ (the parameter η controls the strength of the potential). This transformation converts the resonances into L^2 -integrable wave functions with complex energies

$$E = E_{res} - \frac{i\Gamma}{2}, \quad (4)$$

where the real and imaginary parts correspond to the resonance position (E_{res}) and width (Γ). In a complete basis set, the exact resonance position and width can be recovered in the limit of $\eta \rightarrow 0$. In finite bases, the resonance can only be stabilized at finite values of η . The perturbation due to the finite-strength CAP can be removed by applying first-order de-perturbative correction^{53,54} and identifying the special points of η -trajectories at which the dependence of the computed energy on η is minimal. When combined with the EOM-CCSD ansatz, this approach has been shown to yield accurate and internally consistent results for

both bound and metastable states⁵⁵. For example, these calculations yield smooth potential energy curves⁷⁷⁻⁷⁹ and in many cases correctly identify the points where resonances become bound. We note, however, that in some polyatomic molecules spurious widths of about 0.04 eV for bound states persist⁷⁹. In our previous calculations^{53,55,78-82}, we used CAP-EOM-CCSD to describe metastable EOM states from stable (bound) CCSD references. Here we present the first example of a calculation where the CCSD reference is metastable, but the target EOM-CCSD states are bound.

III. COMPUTATIONAL DETAILS

As explained above, we describe the electronic states of C_2^- and C_2 by EOM-IP-CCSD and EOM-DIP-CCSD, respectively, using the dianionic reference (see Fig. 2). In real-valued EOM-CCSD calculations, we used the aug-cc-pVTZ basis. In the CAP-augmented CCSD and EOM-IP-CCSD calculations, we used the aug-cc-pVTZ+3s3p and aug-cc-pCVTZ+6s6p6d basis sets (the exponents of the additional diffuse sets were generated using the same protocol as in our previous studies^{54,81}). Two core orbitals, σ_{1s} and σ_{1s}^* , were frozen in correlated calculations except when employing the aug-cc-pCVTZ basis. In the calculations using aug-cc-pVTZ+3s3p, the CAP onset was set according to the expectation value of R^2 of the triplet UHF wave function of C_2 (at $r_{cc}=1.28$ Å, this gives the following onsets: $x_0 = y_0=1.6$ Å, $z_0= 2.6$ Å). In the calculations with aug-cc-pCVTZ+6s6p6d, the CAP onset was set according to the expectation value of R^2 of the dianion computed using CCSD/aug-cc-pCVTZ (at $r_{cc}=1.2761$ Å, this gives $x_0 = y_0= 2.4$ Å, $z_0= 3.6$ Å). First-order correction⁵³ was applied to the computed total energy and then optimal values of η were determined from these corrected trajectories using our standard protocol^{53,54}. All electronic structure calculations were carried out using the Q-Chem package^{83,84}. The calculations of partial widths were carried out using ezDyson⁸⁵.

IV. RESULTS AND DISCUSSION

A. C_2

Fig. 3 shows the potential energy curves of low-lying singlet and triplet states of C_2 computed using EOM-DIP-CCSD/aug-cc-pVTZ. The respective electronic configurations,

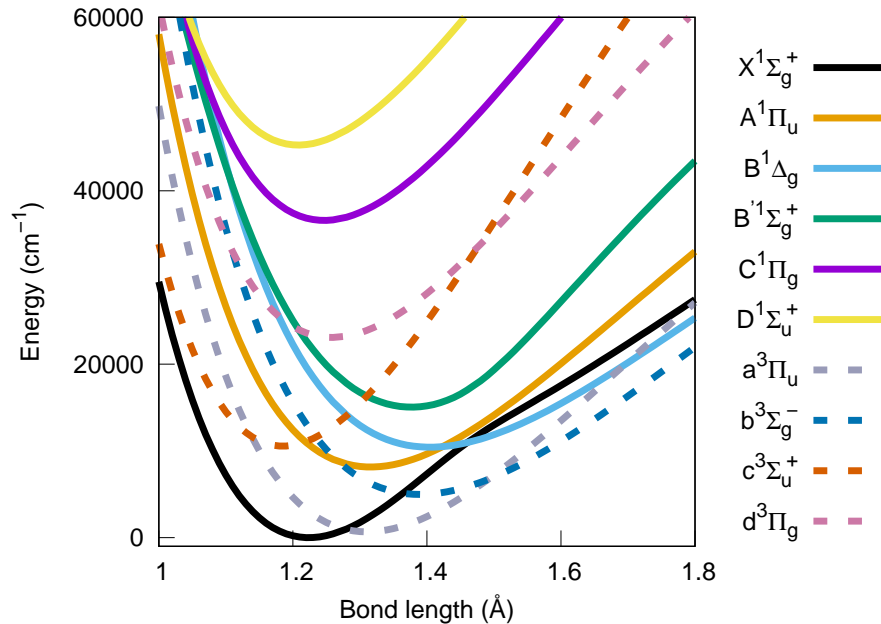


FIG. 3: Potential energy curves of low-lying singlet and triplet states of C_2 .

equilibrium distances, and term values are summarized in Table I. Table I also presents MR-CISD+Q/cc-pVTZ results from Ref. 34 and the experimental values. As one can see, C_2 features 10 electronic states within $\sim 24,000 \text{ cm}^{-1}$ (about 3 eV).

The results illustrate that EOM-DIP-CCSD is capable of tackling the complexity of C_2 rather well. It describes the entire manifold of the low-lying states with an accuracy comparable to that of much more cumbersome and labor-intensive multi-reference calculations. When compared to the experimental values, the root-mean-square (RMS) errors in the equilibrium bond lengths and term energies computed with EOM-DIP-CCSD/aug-cc-pVTZ are 0.0165 \AA and 1661 cm^{-1} . The errors in bond length are only marginally bigger than those of MR-CISD+Q/cc-pVTZ values (0.0114 \AA). Remarkably, the errors in energy are consistently smaller than a conservative estimate of EOM-CCSD error bars, which is roughly 0.3 eV (2420 cm^{-1}). The relative state ordering is also correctly described. MR-CISD+Q/cc-pVTZ yields, on average, smaller errors in term energies (RMS of 469 cm^{-1}), however, for three out of nine states, the EOM-DIP-CCSD/aug-cc-pVTZ values are closer to the experiment.

For a fair comparison, it is important to stress that the EOM-DIP-CCSD ansatz is very compact and includes only $2h$ and $3h2p$ configurations, whereas in MR-CISD+Q and AQCC, the size-extensivity corrections entail contributions of up to quadruply excited configurations. As with other EOM-CCSD methods, perturbative or explicit inclusion of connected

TABLE I: Equilibrium bond lengths (r_e , Å) and term energies (T_{ee} , cm⁻¹) of the low-lying states of C₂.

State	Configuration	EOM-DIP-CCSD ^a		MR-CISD+Q ^b		Expt. ^c	
		r_e	T_{ee}	r_e	T_{ee}	r_e	T_{ee}
$X^1\Sigma_g^+$	[core] ⁶ (σ_{2s}^*) ² (π_{2p_x}) ² (π_{2p_y}) ²	1.224	-	1.2536	-	1.2425	-
$A^1\Pi_u$	[core] ⁶ (σ_{2s}^*) ² (π_{2p_x}) ² (π_{2p_y}) ¹ (σ_{2p_z}) ¹	1.316	8127	1.3294	8000	1.3184	8391
$B^1\Delta_g$	[core] ⁶ (σ_{2s}^*) ² (π_{2p_x}) ¹ (π_{2p_y}) ¹ (σ_{2p_z}) ²	1.404	10408	1.3972	11684	1.3855	12082
$B'^1\Sigma_g^+$	[core] ⁶ (σ_{2s}^*) ² (π_{2p_x}) ¹ (π_{2p_y}) ¹ (σ_{2p_z}) ²	1.377	15012	1.3897	15134	1.3774	15409
$C^1\Pi_g$	[core] ⁶ (σ_{2s}^*) ¹ (π_{2p_x}) ² (π_{2p_y}) ¹ (σ_{2p_z}) ²	1.246	36489	1.2682	34788	1.2552	34261
$D^1\Sigma_u^+$	[core] ⁶ (σ_{2s}^*) ¹ (π_{2p_x}) ² (π_{2p_y}) ² (σ_{2p_z}) ¹	1.208	45166	1.2521	43810	1.2380	43239
$a^3\Pi_u$	[core] ⁶ (σ_{2s}^*) ² (π_{2p_x}) ² (π_{2p_y}) ¹ (σ_{2p_z}) ¹	1.310	694	1.3228	256	1.3119	716
$b^3\Sigma_g^-$	[core] ⁶ (σ_{2s}^*) ² (π_{2p_x}) ¹ (π_{2p_y}) ¹ (σ_{2p_z}) ²	1.390	4971	1.3786	5794	1.3692	6434
$c^3\Sigma_u^+$	[core] ⁶ (σ_{2s}^*) ¹ (π_{2p_x}) ² (π_{2p_y}) ² (σ_{2p_z}) ¹	1.185	10531	1.2170	9618	1.209	9124
$d^3\Pi_g$	[core] ⁶ (σ_{2s}^*) ¹ (π_{2p_x}) ² (π_{2p_y}) ¹ (σ_{2p_z}) ²	1.258	23025	1.2777	20382	1.2661	20022

^a aug-cc-pVTZ basis set.

^b MR-CISD with Davidson correction using the cc-pVTZ basis set from Ref. 34.

^c From Refs. 9–14.

triple excitations is expected to significantly reduce the errors. We note that higher excitations can also describe orbital relaxation thus mitigating the effect of an unstable dianionic reference.

To put the results presented in Table I in a perspective, it is instructive to compare the performance of various flavors of multireference methods and to discuss the effects of basis set increase and higher-order corrections. Szalay *et al.* carried out³⁴ extensive comparisons between MR-CISD, MR-CISD+Q, and MR-AQCC for thirteen states of C₂. The effects of higher-order corrections have also been investigated by Jiang and Wilson³¹ in the framework of the correlation consistent composite approach (MR-ccCA) based on the complete active space self-consistent field (CASSCF) theory with second-order perturbative corrections (CASPT2).

The size-extensivity correction is significant—the errors of MR-CISD decrease when either Davidson’s correction or MR-AQCC is employed. Without size-extensivity corrections,

the RMS in the equilibrium bond lengths and term energies computed with MR-CISD/cc-pVTZ are 0.0117 Å and 623 cm⁻¹. The effect of the basis set on the term energies is less systematic³⁴. The RMS error in bond lengths within MR-AQCC/cc-pVTZ is 0.0115 Å (to be compared to 0.0114 Å of MR-CISD+Q). The errors in term energies were also comparable to MR-CISD+Q/cc-pVTZ. We note that in the MR-AQCC(TQ) calculations, the largest errors in term energies were observed for ¹Δ_u and ^e3Π_g (999 cm⁻¹ and 722 cm⁻¹). Both MR-AQCC and MR-CISD+Q calculations were sensitive to the orbital choice and showed improved performance when using state-averaged CASSCF orbitals. Extrapolation to the complete basis set based on the cc-pVTZ and cc-pVQZ calculations results in a systematic decrease of equilibrium bond lengths by 0.01 Å.

Several studies have also investigated the magnitude of higher-order corrections, with an aim to achieve spectroscopic accuracy^{31,86}. Schmidt and co-workers showed that the inclusion of core-valence correlation combined with scalar relativistic corrections in the framework of MR-CISD+Q brings the spectroscopic constants within 1% from the experimental values³³. Jiang and Wilson have reported similar trends³¹.

In addition to the states shown in Table I, we also computed two electronic states, ¹Δ_u and ^e3Π_g, which have been recently identified experimentally¹⁵⁻¹⁷. The electronic configurations of these states are: [core]⁶(σ_{2s}^{*})²(π_{2p_x})²(π_{2p_y})¹(π_{2p_x}^{*})¹ and [core]⁶(σ_{2s}^{*})²(π_{2p_x})¹(π_{2p_y})¹(σ_{2p_z})¹(π_{2p_x}^{*})¹. Thus, they cannot be generated by the 2*h* operator from the dianionic reference and the norm of the 3*h*1*p* EOM amplitudes becomes large (≈1). Consequently, the computed term energies are too high. In order to describe these states with the same accuracy as the states dominated by 2*h* configurations, the EOM-DIP ansatz needs to be extended up to 4*h*2*p* operators.

We note that several lowest state of C₂ can also be described by EOM-SF-CCSD using a high-spin triplet reference, e.g., [core]⁶(σ_{2s}^{*})²(π_{2p_x})²(π_{2p_y})¹(σ_{2p_z})¹. Using ROHF-EOM-SF-CCSD/aug-cc-pVTZ, vertical excitation energy from ¹Σ_g⁺ to a³Π_u at *r*_{cc}=1.2425 of C₂ is 319 cm⁻¹, to be compared with 1924 cm⁻¹ computed by EOM-DIP-CCSD/aug-cc-pVTZ. To quantify the bonding pattern in C₂, we also computed Head-Gordon's index⁸⁷, which characterizes the number of effectively unpaired electrons. For the EOM-SF-CCSD wave function of the ground state of C₂ at equilibrium, *n*_{u,nl}=0.29. This value indicates that C₂ has substantial diradical character, comparable⁶³ to that of singlet methylene (0.25) or meta-benzyne (0.26). In other words, there is no support for a quadruple bond, which would

be manifested by $n_{u,nl} \approx 0$.

B. C_2^-

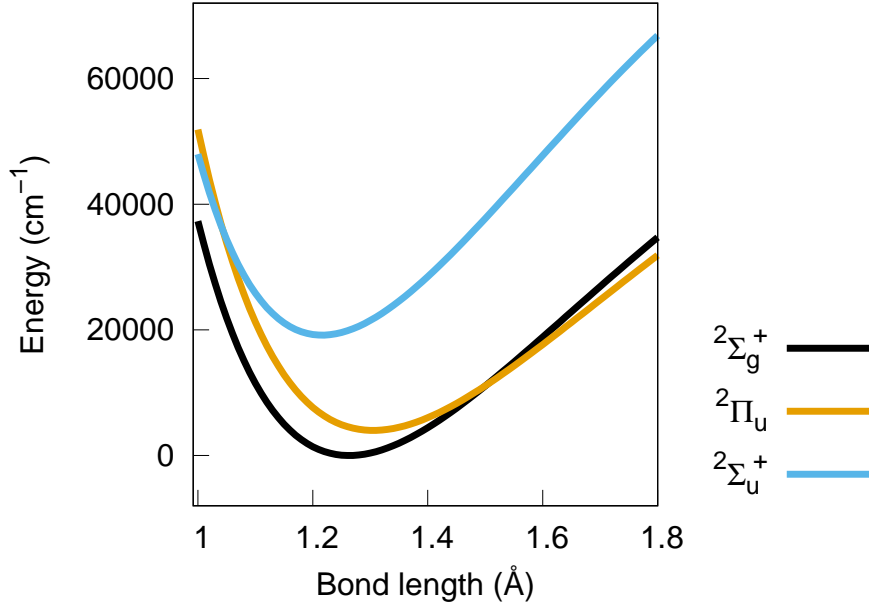


FIG. 4: Potential energy curves of the three lowest states of C_2^- .

TABLE II: Equilibrium bond lengths (r_e , Å) and term energies (T_{ee} , cm^{-1}) of bound electronic states of C_2^- . EOM-IP-CCSD vertical excitation energies (E_{ex} , cm^{-1}) and oscillator strengths (f_l) are also shown.

State	Configuration	EOM-IP-CCSD/aug-cc-pVTZ				Expt. ^a	
		r_e	T_{ee}	E_{ex}	f_l	r_e	T_{ee}
$2\Sigma_g^+$	$[\text{core}]^6(\sigma_{2s}^*)^2(\pi_{2p_x})^2(\pi_{2p_y})^2(\sigma_{2p_z})^1$	1.260				1.268	
$2\Pi_u$	$[\text{core}]^6(\sigma_{2s}^*)^2(\pi_{2p_x})^2(\pi_{2p_y})^1(\sigma_{2p_z})^2$	1.310	3989	4575	0.004	1.308	3986
$2\Sigma_u^+$	$[\text{core}]^6(\sigma_{2s}^*)^1(\pi_{2p_x})^2(\pi_{2p_y})^2(\sigma_{2p_z})^2$	1.219	19113	19801	0.085	1.223	18391

^a From Ref. 88.

Fig. 4 shows the potential energy curves of the three bound states of C_2^- computed using EOM-IP-CCSD/aug-cc-pVTZ. The respective electronic configurations, equilibrium distances, and term values are given in Table II. The Dyson orbitals⁸⁹ representing the unpaired electron in C_2^- are shown in Fig. 1.

As one can see, the computed equilibrium distances and term energies are in excellent agreement with the experimental data. The computed oscillator strengths show that transitions to both excited states are optically allowed. The computed T_{ee} of the ${}^2\Sigma_u^+ \rightarrow {}^2\Sigma_g^+$ transition is 2.37 eV. Vertically, at the equilibrium geometry of the ${}^2\Sigma_u^+$ state, the energy gap between two states is 2.29 eV, which is exactly equal to the fluorescence signal observed in Ref. 21. Thus, our results confirm that fluorescence observed in Ref. 21 can be attributed to the ${}^2\Sigma_u^+ \rightarrow {}^2\Sigma_g^+$ transition of C_2^- .

We also computed adiabatic electron affinity, AEA, of C_2 . Using EOM-DIP-CCSD/aug-cc-pVTZ total energy of $X^1\Sigma_g^+$ and EOM-IP-CCSD/aug-cc-pVTZ total energy of the $X^2\Sigma_g^+$ state at the respective r_e , the computed value of AEA is 4.57 eV (without zero-point energy), which is more than 1 eV larger than the experimental value^{38,39} of 3.27 eV and high-level ab initio estimates⁴⁰. This suggests that the current correlation level is insufficient to describe relative position of the two manifolds. The two relevant states, $X^1\Sigma_g^+$ and ${}^2\Sigma_g^+$, can also be computed using an alternative EOM-CC scheme, via SF and EA using the high-spin triplet reference, $[\text{core}]^6(\sigma_{2s}^*)^2(\pi_{2p_x})^2(\pi_{2p_y})^1(\sigma_{2p_z})^1$. These calculations yield AEA of 3.44 eV when using UHF triplet reference and 3.42 eV when using the ROHF reference. The analysis of the total energies shows that the EOM-EA energy of the anion is very close to the corresponding EOM-IP energy whereas the EOM-SF energy of the neutral state is significantly lower than the EOM-DIP energy. We attribute this to orbital relaxation effects—while the dianionic orbitals are reasonably good for the anion, they are too diffuse for the neutral and the EOM-DIP ansatz with only $2h$ and $3h1p$ operators is not sufficiently flexible to account for that.

C. C_2^{2-}

Fig. 5 shows potential energy curves of C_2^{2-} and C_2^- , clearly illustrating the metastable nature of C_2^{2-} . Adiabatically, C_2^{2-} is 3.41 eV (at the EOM-IP-CCSD/aug-cc-pVTZ level) above the ground state of C_2^- and can decay into any of the 3 states of the anion. The squared norms of the respective Dyson orbitals⁸⁹ computed using the EOM-IP-CCSD/aug-cc-pVTZ wave functions at the equilibrium bondlength of C_2^{2-} (1.28 Å) are 0.86, 0.80, and 0.86 for the ${}^2\Sigma_g^+$, ${}^2\Pi_u$, and ${}^2\Sigma_u^+$ states, respectively. These values indicate that each of these channels corresponds to a one-electron detachment process.

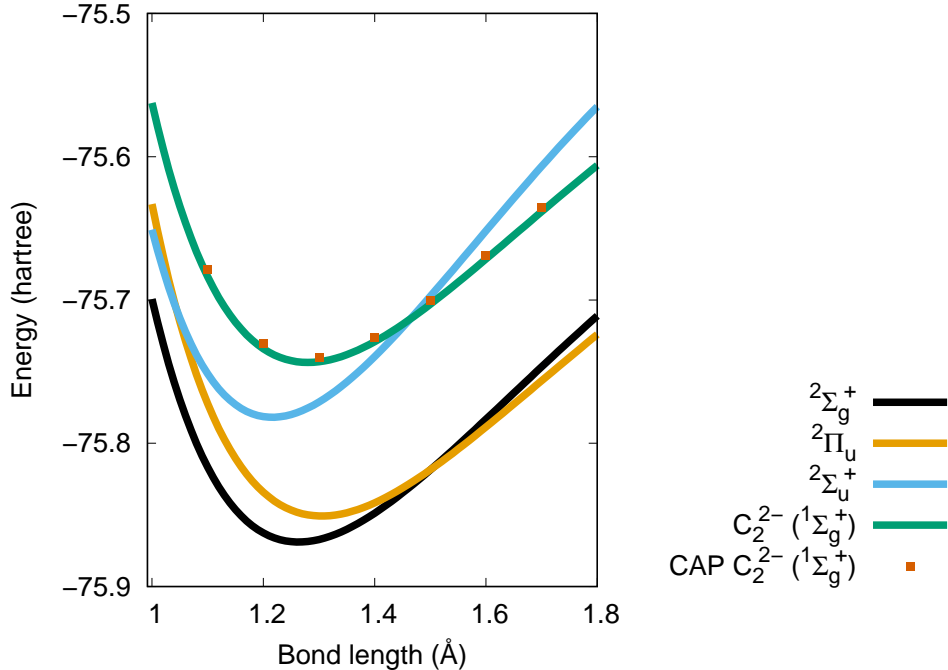


FIG. 5: Potential energy curves of C_2^{2-} and C_2^- . Total electronic energies are shown. Solid lines show CCSD/aug-cc-pVTZ and EOM-IP-CCSD energies. Orange squares show the results from CAP-CCSD/aug-cc-pvTZ+3s3p (first-order corrected energy).

To characterize lifetimes of the dianion and to quantify the effect of its resonance character on the computed quantities of C_2^- , we carried out CAP-CCSD and CAP-EOM-IP-CCSD calculations. The results are summarized in Tables III and IV and shown in Figs. 5 and 6.

As one can see from Fig. 5, the total energies of C_2^{2-} obtained from the CAP-augmented calculations are nearly identical to the real-valued results. Moreover, the impact on the computed term energies of C_2^- is also small: at $r_{CC}=1.28$ Å, the differences in excitation energies of C_2^- between the two calculations are ~ 0.03 eV. The adiabatic energy gap between C_2^{2-} and C_2^- is 3.16 eV computed with CAP-CCSD/aug-cc-pCVTZ+6s6p6d, only slightly smaller than the value obtained in real-valued calculations (3.41 eV).

Previous calculations using the charge-stabilization method⁴³ estimated the closed-shell $^1\Sigma_g^+$ resonance of C_2^{2-} below 4 eV, roughly at around 3.4 eV, above the ground state of C_2^- . Later, CAP-augmented MR-CISD calculations⁴⁴ yielded $E_{res}=3.52$ eV and an equilibrium bond length of 1.285 Å. Thus, our results confirm the findings of these earlier studies^{43,44}.

The resonance position and width are rather sensitive to the basis set employed, as Table III illustrates. For example, at the equilibrium bond length ($r_{CC}=1.28$ Å), the aug-

cc-pVTZ+3s3p basis yields adiabatic $E_{res}=3.7$ eV and $\Gamma=0.68$ eV, whereas the aug-cc-pCVTZ+6s6p6d basis produces $E_{res}=3.16$ eV and $\Gamma=0.25$ eV. A distinct stabilization point of the η -trajectory is only obtained using the larger basis set (see Fig. 6); in the small basis only first-order corrected trajectory shows stabilization point. Our best value for the resonance width (0.25 eV) is in very good agreement with the CAP-MR-CISD value (0.30 eV)⁴⁴ and also agrees qualitatively with the estimate from charge-stabilization calculations (0.26-0.55 eV)⁴³. Compared to singlet resonances with open-shell character, for example those of CN^- that have $\Gamma=0.48$ -0.56 eV⁸¹, C_2^{2-} is a narrow resonance. On the other hand, it is rather broad compared to other small dianions⁶⁹, such as CO_3^{2-} or SO_4^{2-} .

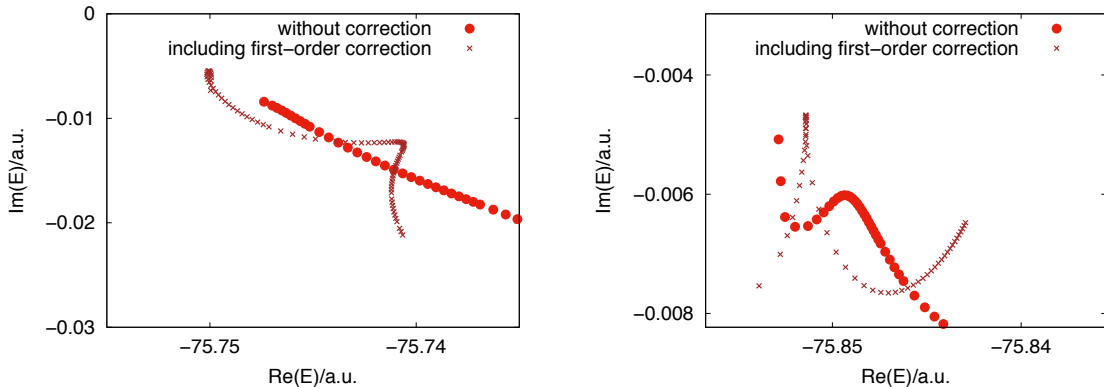


FIG. 6: Uncorrected and first-order corrected CAP-CCSD using aug-cc-pCVTZ+3s3p (left) and aug-cc-pCVTZ+6s6p6d (right) η -trajectories for C_2^{2-} at equilibrium bondlengths.

We also estimated partial widths corresponding to the three decay channels. Within Feshbach formalism, partial widths of autodetachment can be approximated by the following matrix element⁸²:

$$\Gamma_c = \left(2\pi \langle \xi_{\omega_c} | \hat{F} | \phi_c^d \rangle \right)^2, \quad (5)$$

where Γ_c is the partial width corresponding to detachment channel c , ω_c and ϕ_c^d are the respective detachment energy and Dyson orbital, ξ_{ω_c} is the wave function of the free electron, and \hat{F} is the Fock operator. Given the localized nature of \hat{F} , this matrix element is bound by the value of the overlap between the Dyson orbital and the free-electron wave function. Thus, branching ratios x_p corresponding to different detachment channels can be estimated as follows:

$$x_p = \frac{\langle \xi_{\omega_p} | \phi_p^d \rangle^2}{\sum_c \langle \xi_{\omega_c} | \phi_c^d \rangle^2}, \quad (6)$$

giving rise to $\Gamma_p = x_p \Gamma$. Note that the contributions from the degenerate channels (such as Π_u) should be multiplied by the respective degeneracy number (2 for Π -states). The overlap $\langle \xi_{\omega_p} | \phi_p^d \rangle^2$ is proportional to the norm of ϕ_c^d and is strongly dependent on the energy of the detached electron and the shape of the Dyson orbital. Fig. 7 shows the energy dependence of the computed values of the squared overlap between the normalized Dyson orbitals and the free-electron wave function approximated by the Coulomb wave. As one can see, the overlap values are zero at low detachment energies and increase at higher energies. The trends for the Σ_u and Π_u channels are very similar, which is not surprising given the similar shape of the respective Dyson orbitals. Fig. 7 immediately suggest that the autodetachment process will be dominated by the channels producing the two lowest states of the anion, Σ_g and Π_u .

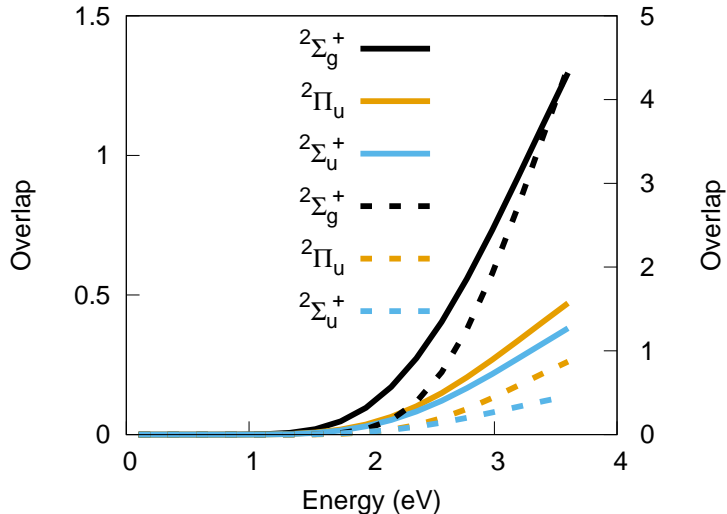


FIG. 7: Squared overlap between Dyson orbitals and a Coulomb wave with charge=-1. Solid line correspond to Dyson orbitals from EOM-IP-CCSD/aug-cc-pVTZ (scale on the left). Dashed lines correspond to Dyson orbitals (real part) from CAP-EOM-IP-CCSD/aug-cc-pVTZ+6s6p6d (scale on the right).

Table ?? lists the computed values using $E_{res}=3.41$ eV (from EOM-IP-CCSD/aug-cc-pVTZ). As one can see, the contribution of the Σ_u is negligible and the Σ_g channel is dominant. When using lower energy value (3.16 eV, from CAP-EOM-IP-CCSD/aug-cc-pCVTZ+6s6p6d), the contribution from the Σ_u channels drops even further while the ratio between the Σ_g and Π_u channels remains unchanged. Using Dyson orbitals from

the CAP-EOM-IP-CCSD/aug-cc-pCVTZ+6s6p6d calculations leads to the increase of the relative weight of the Σ_g channel. These simple estimates are in qualitative agreement with partial widths computed using CAP-MR-CISD wave function and an approach based on CAP projection⁴⁴; their reported values correspond to x_p of 0.31, 0.66, and 0.02 for the Σ_g , Π_u , and Σ_u channels. One important difference is that our calculations predict that the dominant decay channel is Σ_g , producing the ground-state of C_2^- . We note that using plane wave to describe the state of the free electron yields an entirely different picture: the overlaps are rather large around the threshold and change much slower, resulting in comparable branching ratios for all three channels.

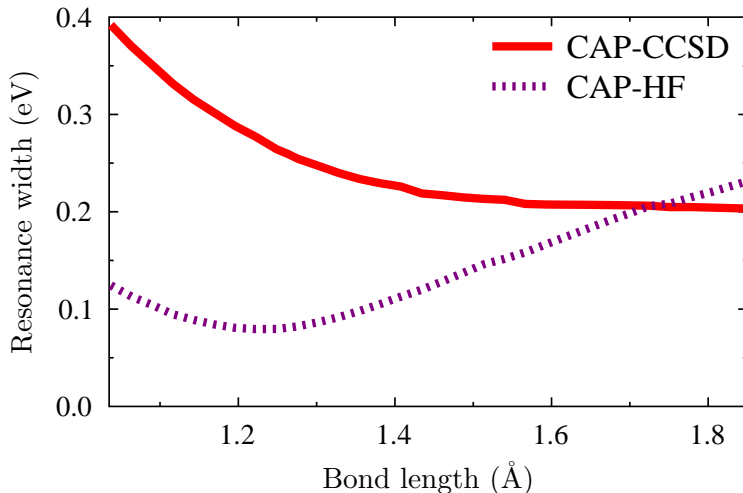


FIG. 8: First-order corrected resonance width of C_2^{2-} as a function of bond length computed with CAP-CCSD and CAP-HF and the aug-cc-pCVTZ+6s6p6d basis set.

Finally, we investigate the dependence of the resonance width on the bond length. As illustrated by Figure 8, the CAP-CCSD resonance width shrinks with an increasing bond length near the equilibrium distance while it is nearly constant beyond 1.6 Å. This is consistent with the potential energy curves of C_2^{2-} and the ${}^2\Sigma_g^+$ and ${}^2\Pi_u$ states of C_2^- becoming nearly parallel at elongated bond distances (see Figure 5). However, the behavior is different from that of valence shape resonances in diatomic molecules (for example, H_2^- or N_2^-) that become bound if the bond is stretched somewhat.⁵⁵ It is more reminiscent of dipole-stabilized resonances whose width is also insensitive towards bond length changes.⁸⁰ Figure 8 also shows that the resonance width behaves differently at the CAP-CCSD and CAP-HF

levels. Within the HF approximation, Γ has a minimum around the equilibrium structure (0.08 eV) and grows when the bond is stretched. This behavior is similar to the results reported in Ref. 44 where CAP-CIS and CAP-MR-CISD also yielded Γ increasing with bond length between 1.2 and 1.4 Å. A detailed investigation of these differences is beyond the scope of the present work, but we note that the resonance width of C_2^{2-} has to vanish eventually, when the bond is stretched far enough, because the 4S ground state of C^- obtained in the dissociation limit is stable towards electron detachment.

The description of the decay channels reveals a shortcoming of the CAP-CCSD approach based on a metastable reference. The CAP-EOM-IP-CCSD energies of the three bound states of C_2^- feature sizable positive imaginary parts of more than 0.3 eV (at the equilibrium bond length and optimal η values for the dianionic resonance). This is despite that real parts of absolute CAP-EOM-IP-CCSD energies agree with the CAP-free values within ~ 0.1 eV. Also, it is in stark contrast to the performance of CAP-EOM-CCSD based on bound reference states^{53,54}, where the imaginary energies of bound states typically stay below 0.03 eV. We note that application of the de-perturbative correction^{53,54} does not rectify this problem. This is not surprising as the original analysis of $E(\eta)$ in terms of perturbation theory⁷⁵ was designed for resonances but not bound states. Furthermore, the imaginary energies of the three bound states of C_2^- differ by more than a factor of two so that a single, not state-specific, correction is not realistic. However, since a positive imaginary energy is unphysical and since no stabilization of the η -trajectory is observed for the CAP-EOM-IP-CCSD states, the problem is easily discernible. Importantly, despite this shortcoming, CAP-EOM-CCSD calculations using an unstable reference clearly distinguish bound and metastable states.

Experimentally^{41,42}, the C_2^{2-} resonance manifest itself as a broad feature around 10 eV in electron scattering detachment spectra from C_2^- , however, the interpretation of these spectra in terms of the position of the resonance is not straightforward, as explained by Sommerfeld and co-workers⁴³. We hope that our results will stimulate further experimental efforts to characterize electronic structure of C_2^{2-} .

TABLE III: First-order corrected energies of C_2^{2-} at optimal values of the η parameter and the corresponding trajectory velocities (in a.u.). computed with CAP-CCSD/aug-cc-pVTZ+3s3p.

$r_{CC}/\text{\AA}$	E^{Re}	Γ	η_{opt}	$\eta \left \frac{dE}{d\eta} \right $
1.1	-75.67858	0.02790	0.0176	8.324×10^{-5}
1.2	-75.73037	0.02618	0.0164	2.061×10^{-5}
1.28	-75.74059	0.02506	0.0156	1.250×10^{-4}
1.3	-75.74022	0.02458	0.0148	2.355×10^{-4}
1.4	-75.72646	0.02346	0.0140	2.016×10^{-4}
1.5	-75.70046	0.02302	0.0128	1.104×10^{-4}
1.6	-75.66865	0.02224	0.0120	1.827×10^{-4}
1.7	-75.63523	0.02172	0.0116	1.427×10^{-4}

TABLE IV: First-order corrected energies of C_2^{2-} at optimal values of the η parameter computed with CAP-CCSD/aug-cc-pCVTZ+6s6p6d and CAP-HF/aug-cc-pCVTZ+6s6p6d.

$r_{CC}/\text{\AA}$	CAP-CCSD			CAP-HF		
	E^{Re}	Γ	η_{opt}	E^{Re}	Γ	η_{opt}
1.0372	-75.730907	0.014406	0.0030	-75.298280	0.004573	0.0028
1.0901	-75.786473	0.012892	0.0030	-75.353147	0.003828	0.0026
1.1430	-75.821827	0.011584	0.0030	-75.387436	0.003267	0.0024
1.1959	-75.841880	0.010590	0.0028	-75.406232	0.002968	0.0020
1.2489	-75.850425	0.009711	0.0028	-75.413353	0.002924	0.0018
1.2761	-75.851410	0.009350	0.0028	-75.413483	0.003025	0.0018
1.3018	-75.850542	0.009089	0.0026	-75.411820	0.003178	0.0018
1.3547	-75.844523	0.008589	0.0026	-75.403959	0.003601	0.0018
1.4076	-75.834038	0.008303	0.0024	-75.391521	0.004147	0.0018
1.4605	-75.820500	0.007975	0.0024	-75.375802	0.004719	0.0018
1.5134	-75.804992	0.007837	0.0024	-75.357905	0.005367	0.0018
1.5664	-75.788195	0.007646	0.0024	-75.338755	0.005815	0.0020
1.6193	-75.770789	0.007618	0.0024	-75.318637	0.006414	0.0020
1.6722	-75.753150	0.007604	0.0022	-75.298126	0.007005	0.0020
1.7251	-75.735635	0.007578	0.0022	-75.277573	0.007564	0.0020
1.7780	-75.718455	0.007528	0.0022	-75.257580	0.007895	0.0020
1.8310	-75.701660	0.007486	0.0020	-75.237545	0.008336	0.0020

TABLE V: Calculation of partial widths using Coulomb wave and Dyson orbitals from real-valued and complex-valued EOM-IP-CCSD calculations.

Channel/DE ^a	EOM-IP-CCSD/aug-cc-pVTZ				CAP-EOM-IP-CCSD/aug-cc-pVTZ+6s6p6d			
	$ \phi_d ^2$	Overlap ^b	x_p	Γ_p	$ \phi_d ^2$	Overlap ^b	x_p	Γ_p
$^2\Sigma_g^+/3.41$	0.86	1.12	0.69	0.17	0.73	3.61	0.83	0.21
$^2\Pi_u/2.91$	0.86	0.25	0.31	0.08	0.71	0.39	0.17	0.04
$^2\Sigma_u^+/1.04$	0.80	2.13×10^{-4}	1.4×10^{-4}	~ 0	0.62	1.6×10^{-4}	~ 0	~ 0

^a Adiabatic EOM-IP-CCSD/aug-cc-pVTZ energies (eV).

^b Overlap (squared) is computed between normalized Dyson orbitals and the Coulomb wave with charge=-1 and kinetic energy corresponding to adiabatic detachment energy.

V. CONCLUSION

We reported electronic structure calculations of C_2 , C_2^- , and C_2^{2-} using the CC/EOM-CC family of methods. The results illustrate that EOM-CCSD provides an attractive alternative to MR approaches. The low-lying states of C_2 and C_2^- are well described by EOM-DIP-CCSD and EOM-IP-CCSD using dianionic closed-shell reference (C_2^{2-}), despite its metastable nature.

EOM-DIP-CCSD offers a much simpler computation approach based on a single-reference formalism. In the EOM-DIP calculations, no active space selection is required and the results of the calculations do not depend on the number of states computed, in contrast to state-averaged MR schemes. One does not need to guess what are the electronic configurations of the states to be computed—once the user specifies how many states in each irrep are desired, the algorithm will compute these states.

The electronic structure of C_2^{2-} was characterized by CAP-augmented CCSD. The calculations place the closed-shell C_2^{2-} resonance 3.16 eV adiabatically above the ground state of C_2^- . The computed resonance width is (0.25 eV), which corresponds to a lifetime of 2.6 fs. Importantly, the CAP-augmented calculations yield detachment energies that are very close to the real-valued EOM-CCSD calculations with the aug-cc-pVTZ basis set thus confirming the validity of the results obtained with EOM-DIP-CCSD and EOM-IP-CCSD using the dianion reference.

Acknowledgments: This work has been supported in Los Angeles by the Army Research Office through grant W911NF-16-1-0232 and the Alexander von Humboldt Foundation (Bessel Award to AIK) and in Munich by the German Research Foundation through grant JA2794/1-1 (Emmy Noether program). AIK is also a grateful recipient of the 2019 Simons Fellowship in Theoretical Physics. SG thanks Dr. W. Skomorowski and Dr. K. Nanda for helpful discussions.

-
- ¹ Rzepa, S. Shaik H. S.; Hoffmann, R. One molecule, two atoms, three views, four bonds? *Angew. Chem. Int. Ed.* **2013**, *52*, 3020–3033.
- ² Xu, L. T.; Dunning, Jr., T. H. Insights into the perplexing nature of the bonding in C₂ from generalized valence bond calculations *J. Chem. Theory Comput.* **2014**, *10*, 195–201.
- ³ Shaik, S.; Danovich, D.; Braida, B.; Hiberty, P. C. The quadruple bonding in C₂ reproduces the properties of the molecule *Chem. Eur. J.* **2016**, *22*, 18977–18980.
- ⁴ Frenking, G.; Hermann, M. Comment on "The quadruple bonding in C₂ reproduces the properties of the molecule" *Chem. Eur. J.* **2016**, *22*, 18975–18976.
- ⁵ Shaik, S.; Danovich, D.; Braida, B.; Hiberty, P. C. A response to a comment by G. Frenking and M. Hermann on "the quadruple bonding in C₂ reproduces the properties of the molecule" *Chem. Eur. J.* **2016**, *22*, 18977–18980.
- ⁶ Tchougreeff, A. L.; Dronskowski, R. Two theorems about C₂ and some more *Mol. Phys.* **2016**, *114*, 1423–1444.
- ⁷ de Sousa, D. W. O.; Nascimento, M. A. C. Is there a quadruple bond in C₂? *J. Chem. Theory Comput.* **2016**, *12*, 22342241.
- ⁸ Piris, M.; Lopez, X.; Ugalde, J. M. The bond order of C₂ from a strictly *N*-representable natural orbital energy functional perspective *Chem. Eur. J.* **2016**, *22*, 4109–4115.
- ⁹ Constants of diatomic molecules (data prepared by J.W. Gallagher and R.D. Johnson, III). Huber, K.P.; Herzberg, G. NIST Chemistry WebBook, NIST Standard Reference Database Number 69; Eds. P.J. Linstrom and W.G. Mallard, July 2001, National Institute of Standards and Technology, Gaithersburg MD, 20899 (<http://webbook.nist.gov>).
- ¹⁰ Douay, M.; Nietmann, R.; Bernath, P. F The discovery of two new infrared electronic transitions of C₂: B¹Δ_g-A¹Π_u and B¹Σ_g⁺-A¹Π_u *J. Molec. Spect.* **1988**, *131*, 261–271.
- ¹¹ Goodwin, P. M.; Cool, T. A. Observation of a new electronic state of C₂ by resonance ionization spectroscopy *J. Chem. Phys.* **1988**, *88*, 4548–4549.
- ¹² Davis, P. S.; M. C. Abrams, J. G. Phillips; Rao, M. L. P. Infrared bands of the C₂ Phillips system *JOSA B* **1988**, *5*, 2280–2285.
- ¹³ Bondybey, V. E. Sequential two photon excitation of the C₂ swan transitions and C₂ relaxation dynamics in rare gas solids *J. Chem. Phys.* **1976**, *65*, 2296–2304.

- ¹⁴ Chauville, J.; Maillard, J. P.; Mantz, A. W. The infrared part of the C₂ Phillips system (2.3-0.9 μm) *J. Molec. Spect.* **1977**, *68*, 399–411.
- ¹⁵ Nakajima, M.; Joester, J. A.; Page, N. I.; Reilly, N. J.; Bacskay, G. B.; Schmidt, T. W.; Kable, S. H. Quantum chemical study and experimental observation of a new band system of C₂, $e^3\Pi_g - e^3\Sigma_u$ *J. Chem. Phys.* **2009**, *131*, 044301.
- ¹⁶ Krechkivska, O.; Bacskay, G. B.; Troy, T. P.; Nauta, K.; Kreuzer, T. D.; Kable, S. H.; Schmidt, T. W. Resonance-enhanced 2photon ionization scheme for C₂ through a newly identified band system: $4^3\Pi_g - a^3\Pi_u$ *J. Phys. Chem. A* **2015**, *119*, 12102–12108.
- ¹⁷ Krechkivska, O.; Welsh, B. A.; Bacskay, G. B.; Nauta, K.; Kable, S. H.; Schmidt, T. W. First observation of the $3^3\Pi_g$ state of C₂: Born-Oppenheimer breakdown *J. Chem. Phys.* **2017**, *146*, 134306.
- ¹⁸ Wollaston, W. H. A Method of examining refractive and dispersive powers, by prismatic reflection *Philos. Trans. R. Soc. London* **1802**, *92*, 365–380.
- ¹⁹ Goyette, A. N.; Lawler, J. E.; Anderson, L. W.; Gruen, D. M.; McCauley, T. G.; Zhou, D.; Krauss, A. R. Spectroscopic determination of carbon dimer densities in Ar-H₂-CH₄ Ar-H₂-C₆₀ and plasmas *J. Phys. D: Appl. Phys.* **1998**, *31*, 1975.
- ²⁰ Reilly, N. J.; Schmidt, T. W.; Kable, S. H. *J. Phys. Chem. A* **2006**, *110*, 12355.
- ²¹ Mahoney, E. J. D.; Truscott, B. S.; Ashfold, M. N. R.; Mankelevich, Yu. A. Optical emission from C₂ anions in microwave-activated CH₄/H₂ plasmas for chemical vapor deposition of diamond *J. Phys. Chem. A* **2017**, *121*, 2760–2772.
- ²² Picazzio, E.; deAlmeida, A. A.; Andrievskii, S. M.; Churyumov, K. I.; Luk'yanyk, I. V. A high spectral resolution atlas and catalogue of emission lines of the comet C/2000 WM1 (linear) *Adv. Space Res.* **2007**, *39*, 462–467.
- ²³ Huggins, W. Aus einem schreiben des herrn William Huggins an den herausgeber *Astron. Nachr.* **1868**, *71*, 382–384.
- ²⁴ Crampton, D.; Cowley, A. P.; Humphreys, R. M. Spectroscopic observations of CRL 2688 *Astrophys. J.* **1975**, *198*, L135–L137.
- ²⁵ Hobbs, L. M. Inter-stellar C₂ molecules toward zeta Persei *Astrophys. J.* **1979**, *232*, L175–L177.
- ²⁶ Goebel, J. H.; Bregman, J. D.; Cooper, D. M.; Goorvitch, D.; Langhoff, S. R.; Witteborn, F. C. The C₂H, C₂, and CN electronic absorption bands in the carbon star hd 19557 *Astrophys. J.* **1983**, *270*, 190–199.

- ²⁷ Klochkova, V. G.; Szczerba, R.; Panchuk, V. E. Optical spectrum of the infrared source IRAS 23304+ 6147 *Astronomy Lett.* **2000**, *26*, 88–103.
- ²⁸ Watts, J. D.; Bartlett, R. J. Coupled-cluster calculations on the C₂ molecule and the C₂⁺ and C₂⁻ molecular ions *J. Chem. Phys.* **1992**, *96*, 6073–6084.
- ²⁹ Li, X.; Paldus, J. Singlet-triplet separation in BN and C₂: Simple yet exceptional systems for advanced correlated methods *Chem. Phys. Lett.* **2006**, *431*, 179–184.
- ³⁰ Shi, D.; Zhang, X.; Sun, J.; Zhu, Z. MRCI study on spectroscopic and molecular properties of B¹Δ_g, B¹Σ_g⁺, C¹Π_g, D¹Σ_g⁺, E¹Σ_g⁺ and 1¹Δ_u electronic states of the C₂ radical *Mol. Phys.* **2011**, *109*, 1453–1465.
- ³¹ Jiang, W.; Wilson, A. K. Multireference composite approaches for the accurate study of ground and excited electronic states: C₂, N₂, and O₂ *J. Chem. Phys.* **2011**, *134*, 034101.
- ³² Christiansen, O.; Koch, H.; Jorgensen, P.; Olsen, J. Excitation energies of H₂O, N₂ and C₂ in full configuration interaction and coupled cluster theory *Chem. Phys. Lett.* **1996**, *256*, 185 – 194.
- ³³ Kokkin, D. L.; Bacskay, G. B.; Schmidt, T. W. Oscillator strengths and radiative lifetimes for C₂: Swan, Ballik-Ramsay, Phillips, and d³Π_g ← c³Σ_u⁺ systems *J. Chem. Phys.* **2007**, *126*, 084302.
- ³⁴ Muller, T.; Dallos, M.; Lischka, H.; Dubrovay, Z.; Szalay, P. G. A systematic theoretical investigation of the valence excited states of the diatomic molecules B₂, C₂, N₃ and O₂ *Theor. Chem. Acc.* **2001**, *105*, 227–243.
- ³⁵ Rehfuss, B. D.; Liu, D. J.; Dinelli, B. M.; Jagod, M. F.; Ho, W. C.; Crofton, M. W.; Oka, T. Infrared-spectroscopy of carbo-ions.4. the A²Π – X²Σ_g⁺ electronic-transition of C₂⁻ *J. Chem. Phys.* **1988**, *89*, 129–137.
- ³⁶ Tulej, M.; Knopp, G.; Gerber, T.; Radi, P. P. Degenerate and two-color resonant four-wave mixing of C₂⁻ in a molecular beam environment *J. Raman Spect.* **2010**, *41*, 853–858.
- ³⁷ Gerber, S.; Fesel, J.; Doser, M.; Comparat, D. Photodetachment and Doppler laser cooling of anionic molecules *New J. Phys.* **2018**, *20*, 023024.
- ³⁸ Ervin, K. M.; Lineberger, W. C. Photoelectron spectra of C₂⁻ and C₂H⁻ *J. Phys. Chem.* **1991**, *95*, 1167–1177.
- ³⁹ Arnold, D. W.; Bradforth, S. E.; Kitsopoulos, T. N.; Neumark, D. M. Vibrationally resolved spectra of C₂-C₁₁ by anion photoelectron spectroscopy *J. Chem. Phys.* **1991**, *95*, 8753–8764.

- ⁴⁰ Feller, D. Application of a convergent, composite coupled cluster approach to bound state, adiabatic electron affinities in atoms and small molecules *J. Chem. Phys.* **2016**, *144*, 014105.
- ⁴¹ Andersen, L. H.; Hvelplund, P.; Kella, D.; Mokler, P.; Pedersen, H. B.; Schmidt, H. T.; Vejby-Christensen, L. Resonance structure in the electron-impact detachment cross section of C_2^- caused by the formation of C_2^{2-} *J. Phys. B* **1996**, page L643.
- ⁴² Pedersen, H. B.; Djurić, N.; Jensen, M. J.; Kella, D.; Safvan, C. P.; Vejby-Christensen, L.; Andersen, L. H. Doubly charged negative ions of B_2 and C_2 *Phys. Rev. Lett.* **1998**, *81*, 5302–5305.
- ⁴³ Sommerfeld, T.; Riss, U. V.; Meyer, H.-D.; Cederbaum, L. S. Metastable C_2^{2-} dianion *Phys. Rev. Lett.* **1997**, *79*, 1237–1240.
- ⁴⁴ Sommerfeld, T.; Tarantelli, F.; Meyer, H.-D.; Cederbaum, L. S. Ab initio calculation of energies and lifetimes of metastable dianions: The C_2^{2-} resonance *J. Chem. Phys.* **2000**, *112*, 6635–6642.
- ⁴⁵ Stanton, J. F.; Gauss, J. A discussion on some problems associated with the quantum mechanical treatment of open-shell molecules *Adv. Chem. Phys.* **2003**, *125*, 101–146.
- ⁴⁶ Krylov, A. I. Equation-of-motion coupled-cluster methods for open-shell and electronically excited species: The hitchhiker’s guide to Fock space *Annu. Rev. Phys. Chem.* **2008**, *59*, 433–462.
- ⁴⁷ Sneskov, K.; Christiansen, O. Excited state coupled cluster methods *WIREs Comput. Mol. Sci.* **2012**, *2*, 566–584.
- ⁴⁸ Bartlett, R. J. Coupled-cluster theory and its equation-of-motion extensions *WIREs Comput. Mol. Sci.* **2012**, *2*, 126–138.
- ⁴⁹ Krylov, A. I. In *Reviews in Comp. Chem.*; Parrill, A.L., Lipkowitz, K.B., Eds., Vol. 30; J. Wiley & Sons, 2017.
- ⁵⁰ Sattelmeyer, K. W.; Schaefer, H. F.; Stanton, J. F. Use of 2h and 3h-p like coupled-cluster Tamm-Dancoff approaches for the equilibrium properties of ozone *Chem. Phys. Lett.* **2003**, *378*, 42–46.
- ⁵¹ Stanton, J. F.; Gauss, J. Analytic energy derivatives for ionized states described by the equation-of-motion coupled cluster method *J. Chem. Phys.* **1994**, *101*, 8938–8944.
- ⁵² Pieniazek, P. A.; Bradforth, S. E.; Krylov, A. I. Charge localization and Jahn-Teller distortions in the benzene dimer cation *J. Chem. Phys.* **2008**, *129*, 074104.
- ⁵³ Jagau, T.-C.; Zuev, D.; Bravaya, K. B.; Epifanovsky, E.; Krylov, A. I. A fresh look at resonances and complex absorbing potentials: Density matrix based approach *J. Phys. Chem. Lett.* **2014**,

- 5, 310–315.
- ⁵⁴ Zuev, D.; Jagau, T.-C.; Bravaya, K. B.; Epifanovsky, E.; Shao, Y.; Sundstrom, E.; Head-Gordon, M.; Krylov, A. I. Complex absorbing potentials within EOM-CC family of methods: Theory, implementation, and benchmarks *J. Chem. Phys.* **2014**, *141*, 024102.
- ⁵⁵ Jagau, T.-C.; Bravaya, K. B.; Krylov, A. I. Extending quantum chemistry of bound states to electronic resonances *Annu. Rev. Phys. Chem.* **2017**, *68*, 525–553.
- ⁵⁶ Stanton, J. F.; Bartlett, R. J. The equation of motion coupled-cluster method. A systematic biorthogonal approach to molecular excitation energies, transition probabilities, and excited state properties *J. Chem. Phys.* **1993**, *98*, 7029–7039.
- ⁵⁷ Krylov, A. I. Size-consistent wave functions for bond-breaking: The equation-of-motion spin-flip model *Chem. Phys. Lett.* **2001**, *338*, 375–384.
- ⁵⁸ Krylov, A. I. The spin-flip equation-of-motion coupled-cluster electronic structure method for a description of excited states, bond-breaking, diradicals, and triradicals *Acc. Chem. Res.* **2006**, *39*, 83–91.
- ⁵⁹ Nooijen, M.; Bartlett, R. J. Equation of motion coupled cluster method for electron attachment *J. Chem. Phys.* **1995**, *102*, 3629–3647.
- ⁶⁰ Orms, N.; Krylov, A. I. Modeling photoelectron spectra of CuO, Cu₂O, and CuO₂ anions with equation-of-motion coupled-cluster methods: An adventure in Fock space *J. Phys. Chem. A* **2018**, *122*, 3653–3664.
- ⁶¹ Pokhilko, P.; Shannon, R.; Glowacki, D.; Wang, H.; Krylov, A. I. Spin-forbidden channels in reactions of unsaturated hydrocarbons with O(³P) *J. Phys. Chem. A* **2018**; submitted; <https://doi.org/10.26434/chemrxiv.7230986.v1>.
- ⁶² Orms, N.; Krylov, A. I. Singlet-triplet energy gaps and the degree of diradical character in binuclear copper molecular magnets characterized by spin-flip density functional theory *Phys. Chem. Chem. Phys.* **2018**, *20*, 13095–13662.
- ⁶³ Orms, N.; Rehn, D. R.; Dreuw, A.; Krylov, A. I. Characterizing bonding patterns in diradicals and triradicals by density-based wave function analysis: A uniform approach *J. Chem. Theory Comput.* **2017**, *14*, 638–648.
- ⁶⁴ Nooijen, M.; Bartlett, R. J. Similarity transformed equation-of-motion coupled-cluster theory: Details, examples, and comparisons *J. Chem. Phys.* **1997**, *107*, 6812–6830.
- ⁶⁵ Wladyslawski, M.; Nooijen, M. In *ACS Symposium Series*, pages, 65–92, 2002.

- ⁶⁶ Musiał, M.; Perera, A.; Bartlett, R. J. Multireference coupled-cluster theory: The easy way *J. Chem. Phys.* **2011**, *134*, 114108.
- ⁶⁷ Bartlett, R. J. The coupled-cluster revolution *Mol. Phys.* **2010**, *108*, 2905–2920.
- ⁶⁸ Taatjes, C. A.; Osborn, D. L.; Selby, T. M.; Meloni, G.; Trevitt, A. J.; Epifanovsky, E.; Krylov, A. I.; Sirjean, B.; Dames, E.; Wang, H. Products of the benzene + O(³P) reaction *J. Phys. Chem. A* **2010**, *114*, 3355–3370.
- ⁶⁹ Dreuw, A.; Cederbaum, L. S. Multiply charged anions in the gas phase *Chem. Rev.* **2002**, *102*, 181–200.
- ⁷⁰ Zuev, D.; Bravaya, K. B.; Crawford, T. D.; Lindh, R.; Krylov, A. I. Electronic structure of the two isomers of the anionic form of p-coumaric acid chromophore *J. Chem. Phys.* **2011**, *134*, 034310.
- ⁷¹ Kuś, T.; Krylov, A. I. Using the charge stabilization technique in the double ionization potential equation-of-motion calculations with dianion references *J. Chem. Phys.* **2011**, *135*, 084109.
- ⁷² Kuś, T.; Krylov, A. I. De-perturbative corrections for charge-stabilized double ionization potential equation-of-motion coupled-cluster method *J. Chem. Phys.* **2012**, *136*, 244109.
- ⁷³ Moiseyev, N. *Non-Hermitian quantum mechanics*; Cambridge University Press, 2011.
- ⁷⁴ Jolicard, G.; Austin, E. J. Optical potential stabilisation method for predicting resonance levels *Chem. Phys. Lett.* **1985**, *121*, 106–110.
- ⁷⁵ Riss, U. V.; Meyer, H.-D. Calculation of resonance energies and widths using the complex absorbing potential method *J. Phys. B* **1993**, *26*, 4503–4536.
- ⁷⁶ Cvetanović, R.J. Evaluated chemical kinetic data for the reactions of atomic oxygen O(³P) with unsaturated-hydrocarbons *J. Phys. Chem. Ref. Data* **1987**, *16*, 261–326.
- ⁷⁷ Jagau, T.-C.; Krylov, A. I. Complex absorbing potential equation-of-motion coupled-cluster method yields smooth and internally consistent potential energy surfaces and lifetimes for molecular resonances *J. Phys. Chem. Lett.* **2014**, *5*, 3078–3085.
- ⁷⁸ Benda, Z.; Rickmeyer, K.; Jagau, T.-C. Structure optimization of temporary anions *J. Chem. Theory Comput.* **2018**, *14*, 3468–3478.
- ⁷⁹ Benda, Z.; Jagau, T.-C. Understanding processes following resonant electron attachment: Minimum-energy crossing points between anionic and neutral potential energy surfaces *J. Chem. Theory Comput.* **2018**, *14*, 4216–4223.
- ⁸⁰ Jagau, T.-C.; Dao, D. B.; Holtgrewe, N. S.; Krylov, A. I.; Mabbs, R. Same but different: Dipole-

- stabilized shape resonances in CuF^- and AgF^- *J. Phys. Chem. Lett.* **2015**, *6*, 2786–2793.
- ⁸¹ Skomorowski, W.; Gulania, S.; Krylov, A. I. Bound and continuum-embedded states of cyanopolyne anions *Phys. Chem. Chem. Phys.* **2018**, *20*, 4805–4817.
- ⁸² Skomorowski, W.; Krylov, A. I. Real and imaginary excitons: Making sense of resonance wavefunctions by using reduced state and transition density matrices *J. Phys. Chem. Lett.* **2018**, *9*, 4101–4108.
- ⁸³ Shao, Y.; Gan, Z.; Epifanovsky, E.; Gilbert, A.T.B.; Wormit, M.; Kussmann, J.; Lange, A.W.; Behn, A.; Deng, J.; Feng, X., et al. Advances in molecular quantum chemistry contained in the Q-Chem 4 program package *Mol. Phys.* **2015**, *113*, 184–215.
- ⁸⁴ Krylov, A. I.; Gill, P. M. W. Q-Chem: An engine for innovation *WIREs Comput. Mol. Sci.* **2013**, *3*, 317–326.
- ⁸⁵ ezDyson user’s manual. Gozem, S.; Krylov, A. I. **2015**;
ezDyson, <http://iopenshell.usc.edu/downloads/>.
- ⁸⁶ Peterson, K. A. Accurate multireference configuration interaction calculations on the lowest $^1\Sigma^+$ and $^3\Pi$ electronic states of C_2 , CN^+ , BN , and BO^{+4} *J. Chem. Phys.* **1995**, *102*, 262–277.
- ⁸⁷ Head-Gordon, M. Characterizing unpaired electrons from the one-particle density matrix *Chem. Phys. Lett.* **2003**, *372*, 508–511.
- ⁸⁸ Mead, R. D.; Hefter, U.; Schulz, P. A.; Lineberger, W. C. Ultrahigh resolution spectroscopy of C_2^- : The $\text{A}^2\Pi_u$ state characterized by deperturbation methods *J. Chem. Phys.* **1985**, *82*, 1723–1731.
- ⁸⁹ Oana, C. M.; Krylov, A. I. Dyson orbitals for ionization from the ground and electronically excited states within equation-of-motion coupled-cluster formalism: Theory, implementation, and examples *J. Chem. Phys.* **2007**, *127*, 234106–14.